# Microstructure and hydrogenation properties of RETMMg15 (RE= Nd, Gd; TM= Cu, Ni) alloys

Manuel Legrée, Etienne Gaudin, Jacques Huot, Jean-Louis Bobet

International Journal of Hydrogen Energy xxx (xxxx) xxx

International Journal of Hydrogen Energy

# Microstructure and hydrogenation properties of $RETMMg_{15}$ (RE= Nd, Gd; TM= Cu, Ni) alloys

M. Legrée [a,*], E. Gaudin [a], J. Huot [b], J.-L. Bobet [a]

[a] Bordeaux University, ICMCB, CNRS, UMR 5026, F-33600, Pessac, France
[b] Hydrogen Research Institute, Université du Québec à Trois-Rivières, 3351 Bd des Forges, Trois-Rivières, QC, G9A 5H7, Canada

ARTICLE INFO

Handling editor Ibrahim Dincer

*Keywords:*
Hydrogen storage
Magnesium
Ternary alloys

ABSTRACT

In this study, five $RETMMg_{15}$ (RE = Nd and/or Gd, TM = Ni and/or Cu) alloys have been successfully synthesized by induction melting of pure elements and characterized by XRD, BSE-SEM and EDXS. Their hydrogen storage properties have been studied from kinetic and thermodynamic points of view. The synthesized alloys $NdNiMg_{15}$, $NdCuMg_{15}$ and $GdCuMg_{15}$ were composed of a $RETMMg_{15}$ main phase with lesser proportions of α-Mg phase and other ternary phases. It has been found that substituting half of the RE (or TM) element by another RE (or TM) element leads to the formation of two solid solutions with composition: $Nd_{0.5}Gd_{0.5}CuMg_{15}$ and $NdCu_{0.5}Ni_{0.5}Mg_{15}$. Upon first hydrogenation, all alloys decomposed into binary or ternary hydrides. Next hydrogenation cycles allowed to store reversibly around 4.5 %wt. hydrogen. All alloys presented reduced $MgH_2$ formation enthalpies as compared to pure Mg which is explained in term of "chemical milling".

## 1. Introduction

Dihydrogen is considered as an energy carrier for a green energy economy [1,2]. This molecule has a very attractive weight energy density of 33.6 KWh/Kg. However, because of the low density of its gaseous form (0.09 g/L at 1.013 bar and 273 K), the volumetric energy density ($3.10^{-3}$ KWh/L) under normal conditions of temperature and pressure is very low. It is therefore necessary to find ways to store dihydrogen in a denser form. Physical techniques of hydrogen storage comprise gas compression (40 g/L at 700 bar) and liquefaction (70 g/L at 20 K). The chemical hydrogen storage in metal hydrides is even more interesting in terms of volumetric energy density as it allows to store over 100 g/L depending on the metal/intermetallic used. Nevertheless, it suffers from a low weight capacity (*e.g.* 1.5 wt% for $LaNi_5$). Magnesium is among the lightest metals allowing to store hydrogen under hydride form ($MgH_2$). $MgH_2$ presents a volumetric hydrogen density as high as 110 g/L (7.6 % wt.) that makes it a good candidate for solid hydrogen storage [1,3]. Its use is however limited by slow absorption and desorption kinetics as well as the high stability of the hydride, which imposes to use operating temperatures above 300 °C. Such high temperatures narrow its applicability and reduce the storage efficiency. In order to address these issues, researchers have explored several options. For instance, mechanical activation of the surfaces allows increasing the reaction kinetics by creating defects in the structure through which hydrogen can diffuse easily [4,5]. Alloying Mg with transition metals and/or Rare earth is also considered in order to modify the thermodynamic equilibrium of the system as well as influencing the reaction kinetics [6–13]. For instance, $GdNi_4Mg$ absorbs hydrogen reversibly at room temperature [14]. But in such compound, as the Mg content is low, the gravimetric capacity is limited. In order to get better capacities, ternary compounds with higher Mg content must be considered.

Alasmar et al. have presented $NdNiMg_{15}$ intermetallic for the first time in 2018 as the Mg richest compound ever reported in the Nd-Ni-Mg system [15]. The structure described consists in a three-dimensional framework of magnesium atoms with channels filled by one-dimensional chain consisting of alternating Nd and Ni atoms along the c-axis. This kind of material is interesting for hydrogen storage since Nd and Ni elements are homogeneously distributed in the Mg network. These features may result in high gravimetric capacity along with reduced desorption temperatures.

In this work, $NdNiMg_{15}$ as well as four other $RETMMg_{15}$ (RE = Nd or Gd and TM = Ni or Cu) compounds have been synthesized by induction melting of pure elements and characterized by XRD, BSE-SEM and EDXS. Their hydrogen storage properties have been studied through absorption, desorption and Pressure-Composition-Temperature (PCT) measurements at different temperatures. The effect of alloying elements (Nd,

* Corresponding author.
*E-mail address:* manuel.legree@gmail.com (M. Legrée).

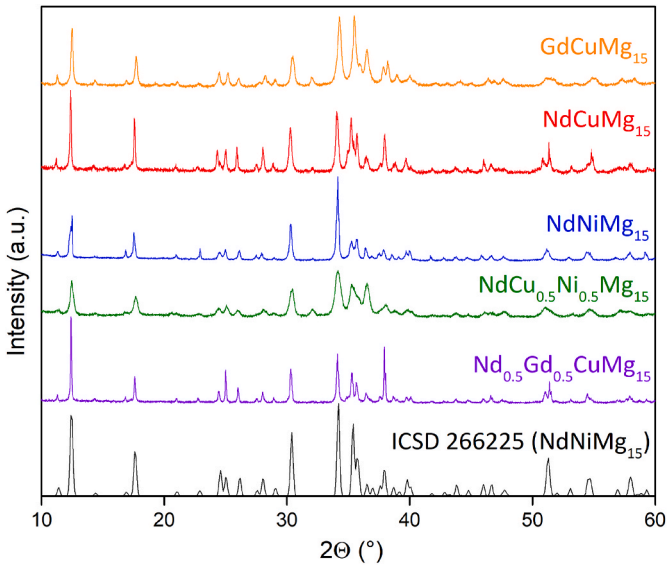


**Fig. 1.** X-Ray diffraction patterns (λ = 1.5406 Å) acquired on powders of the 5 studied alloys and comparison with calculated $NdNiMg_{15}$ (black).

Gd, Ni and Cu) on alloys microstructure and hydrogen storage properties is discussed.

## 2. Materials and methods

The compounds involved in the present study were synthesized using chunks of magnesium (sigma), copper, nickel, gadolinium and neodymium (Strem chemicals, all purities are higher than 99.9 %). The elements were sealed in tantalum crucible under low Argon atmosphere to avoid Mg evaporation during induction melting. All the obtained ingots (in the Ta tube) were subsequently annealed under argon atmosphere at 600 °C for 10 days followed by air-cooling. Samples were crushed in a glovebox under Ar atmosphere for XRD and hydrogen sorption measurements. For SEM analysis, samples were polished up to grit 4000 using ethanol as a lubricant.

Samples were systematically characterized by powder X-ray diffraction (XRD) using a Bruker D8 Focus diffractometer with Cu Kα1 radiation (λ = 1.5406 Å). Scanning Electron Microscopy (SEM) observations were made using an ITACHI SU1510 microscope equipped with secondary electron and back scattered electron detectors (hereafter referred to as SE and BSE modes respectively). Furthermore, the elemental composition of the surface was analyzed using an energy dispersive X-ray (EDXS) detector from Oxford instruments. The hydrogen sorption properties were measured using a homemade Sievert's apparatus.

## 3. Results and discussion

### 3.1. Material characterization

The X-Ray Diffractograms (XRD) of the five studied materials are presented on Fig. 1 as well as the simulated pattern of $NdNiMg_{15}$ phase calculated by using crystallographic data from Alasmar et al. [15]. It appears clearly from this figure that all five composition formed a $RETMMg_{15}$ phase. To our knowledge, $RETMMg_{15}$ phases are reported here for the first time with RE = Nd and TM = Cu. Moreover, it seems to indicate that this phase can be formed by substituting half of the RE (or TM) elements by another RE (or TM) as $NdCu_{0.5}Ni_{0.5}Mg_{15}$ and $Nd_{0.5}Gd_{0.5}CuMg_{15}$ both show a diffraction pattern corresponding to that of $NdNiMg_{15}$ structure. It is important to note that 1-1-15 is a new phase that had been synthesized only with TM = Ni and RE = Nd before the present work. Here, it is shown that the phase can also form with TM = Cu and RE = Gd and that intermediate phases also exist. The relative intensities of the peaks are different among the compositions. This variation is influenced by the nature of the elements involved in the phase but also by the preferential orientation induced when preparing the sample for XRD analysis and crushing soft Mg-rich samples that easily form flake-like particles. The crystallite size calculated by scherrer-Laue Law is 0,4 for NdNiMg15 and NdCuNiMg15, 0,5 for GdCuMg15 and 1,1 for NdCuMg15 and NdGdCuMg15.

Scanning Electron Microscopy (SEM) with BackScattered Electron (BSE) detection mode was performed on the samples in order to complete the characterization of the materials (Fig. 2). The images obtained show three distinct chemical contrast. Energy Dispersive X-ray Spectroscopy (EDXS) was used to identify the chemical composition of these different regions. The compositions measured are reported in Table 1 along with the surface proportions deduced from BSE images analysis. In all alloys, the main region (intermediate brightness on Fig. 2) has a composition close to $RE_{5.9}TM_{5.9}Mg_{88.2}$, which is the stoichiometry of $RETMMg_{15}$ phase. This observation confirms the XRD results, evidencing the formation of $RETMMg_{15}$ phases with various RE and TM chemical elements. In particular, $NdCu_{0.5}Ni_{0.5}Mg_{15}$ shows shared proportions between TM elements: Cu = 3.4%at. and Ni = 3.2%at. In the same way for $Nd_{0.5}Gd_{0.5}CuMg_{15}$, RE elements are equally present in the phase (with Nd = 3%at. and Gd = 3.3%at.). These measurements confirm the possibility of forming intermediary phases (*i.e.* solid solution) of the $NdNiMg_{15}$-type by substituting part of the TM or RE elements. The other regions identified correspond to α-Mg phase (darkest region on Fig. 2) and other ternary (quaternary when two TM or two RE) compositions (brightest region on Fig. 2). The presence of magnesium as secondary phase can be observed on the diffraction pattern at around 32° (the (100) peak is observed for α-Mg at 2θ = 32.2°). The relative ratio between the main phase and α-Mg seems sometimes quite far from the one reported in Table 1 (SEM analysis). For instance, the amount of α-Mg in the $Nd_{0.5}Gd_{0.5}CuMg_{15}$ sample looks much lower from the XRD pattern than the value determined from BSE. The XRD analysis should however be more representative of the whole sample than local micrograph, which indicates that the amount of secondary phases is small in the studied samples.

### 3.2. Hydrogenation

#### 3.2.1. Activation

The alloys were activated during 15 h (until stabilization of pressure) under 2000 kPa of $H_2$ at 623 K. This procedure resulted in the decomposition of the initial phases into different hydrides, namely $MgH_2$, $REH_{2+x}$ and $Mg_xTM_yH_z$. After hydrogenation, all XRD patterns show the disappearance of the initial $RETMMg_{15}$ phase. This result is similar to other Mg-rich compounds found in the literature [7,11,16,17]. Fig. 3 illustrates this point with $NdCuMg_{15}$ XRD patterns acquired at different stages of hydrogenation. It shows that after activation step (red pattern), all peaks related to $NdCuMg_{15}$ phase disappeared and turned to $MgCu_2$, $MgH_2$ and $NdH_{2+x}$ phases formed according to the following reaction:

$$2\ NdCuMg_{15} + (31 + x)\ H_2 \text{-} > 29MgH_2 + 2\ NdH_{2+x} + MgCu_2\ (0 < x < 1) \quad (1)$$

Upon dehydrogenation, $MgCu_2$ transforms into $Mg_2Cu$ in the early stage of the reaction (purple pattern) and $MgH_2$ turns progressively into metallic Mg while stable $NdH_{2+x}$ is still present. Neglecting the stable rare earth hydride, two desorption reactions can be identified:

$$MgH_2 \text{-} > Mg + H2 \quad (2)$$

$$MgCu2 + 3\ MgH_2 \text{-} > 2Mg_2Cu + 3\ H_2 \quad (3)$$

When the TM involved was Ni, the formation of $Mg_2NiH_x$ was identified by XRD (Cf. supplementary materials), showing that the following reaction occurs during first activation:

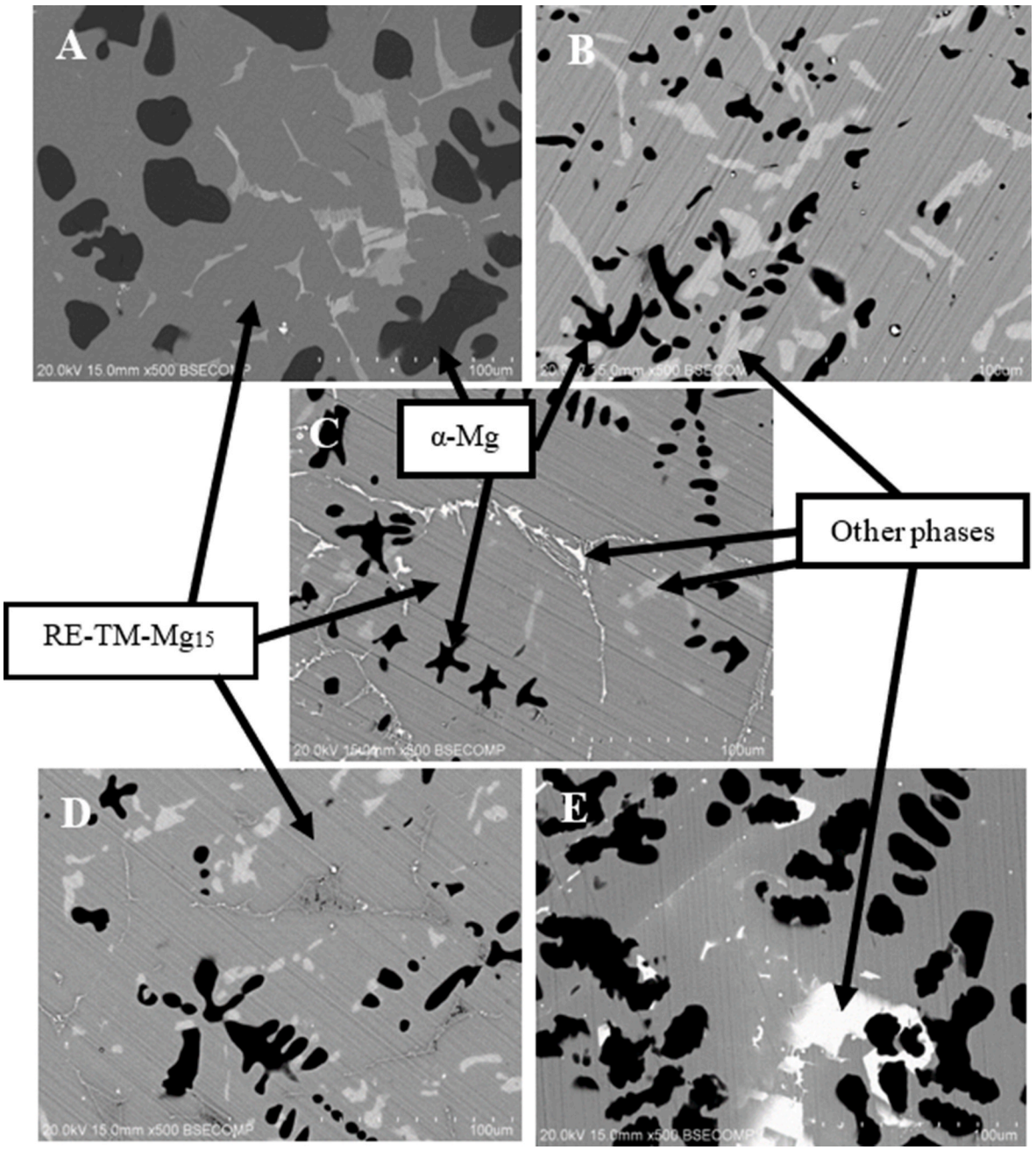


**Fig. 2.** BSE-SEM micrographs of: A-$GdCuMg_{15}$, B- $NdCuMg_{15}$, C- $NdNiMg_{15}$, D- $NdCu_{0.5}Ni_{0.5}Mg_{15}$ and E– $Nd_{0.5}Gd_{0.5}CuMg_{15}$.

**Table 1**
Characterization features obtained from BSE-SEM and EDXS analysis.

| Alloy | Main region composition (EDXS) | Surface proportion of main phase ($RETMMg_{15}$) | Surface proportion of α-Mg phase (dark region on BSE-SEM) | Other regions (EDXS) | Surface proportion of other regions (bright phases on BSE-SEM) |
|---|---|---|---|---|---|
| $GdCuMg_{15}$ ($Gd_{5.9}Cu_{5.9}Mg_{88.2}$) | $Gd_{6.2}Cu_{7.4}Mg_{86.4}$ | 80 % | 16 % | $Gd_{10.2}Cu_{16.6}Mg_{73.2}$ | 4 % |
| $NdCuMg_{15}$ ($Nd_{5.9}Cu_{5.9}Mg_{88.2}$) | $Nd_{6.5}Cu_{6.5}Mg_{87.0}$ | 74 % | 10 % | $Nd_{8.3}Cu_{3.2}Mg_{88.5}$ | 16 % |
| $NdNiMg_{15}$ ($Nd_{5.9}Ni_{5.9}Mg_{88.2}$) | $Nd_{6.1}Ni_{5.7}Mg_{88.2}$ | 89 % | 6 % | $Nd_{8.2}Ni_{1.7}Mg_{90.1}$ - $Nd_{10}Ni_{15}Mg_{75}$ | 3 % and 2 % respectively |
| $NdCu_{0.5}Ni_{0.5}Mg_{15}$ ($Nd_{5.9}Cu_{2.95}Ni_{2.95}Mg_{88.2}$) | $Nd_{6.6}Cu_{3.4}Ni_{3.2}Mg_{86.8}$ | 87 % | 9 % | $Nd_{8.5}Cu_{1.7}Ni_{1.0}Mg_{87.7}$ | 4 % |
| $Nd_{0.5}Gd_{0.5}CuMg_{15}$ ($Nd_{2.95}Gd_{2.95}Cu_{5.9}Mg_{88.2}$) | $Nd_{3.0}Gd_{3.3}Cu_{6.0}Mg_{87.7}$ | 60 %* | 35 %* | $Nd_{1.6}Gd_{11.8}Cu_{1.6}Mg_{85.0}$ | 5 % |

(*) These values seems high considering the XRD pattern, it is probably due the local nature of SEM analysis, which may not be fully representative of the whole sample.

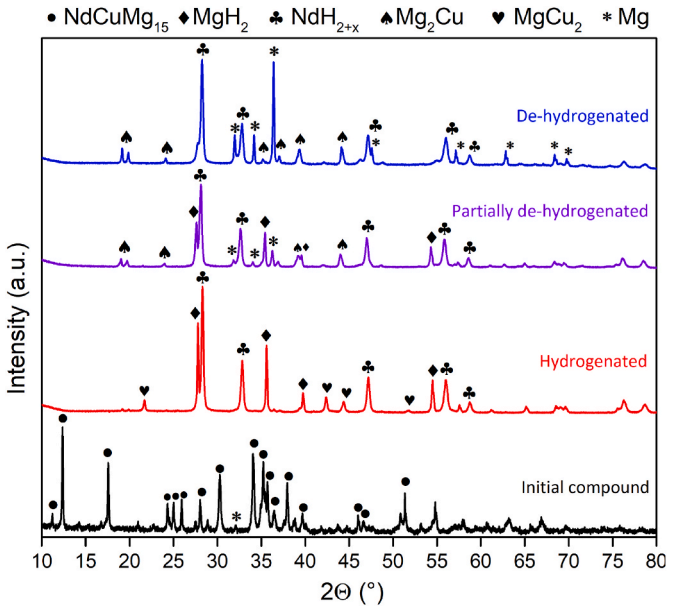


**Fig. 3.** X-ray diffractograms on powder at different stages of hydrogenation (350 °C, 2000 KPa) for $NdCuMg_{15}$.

$$NdNiMg_{15} + (14 + x)\ H_2 -> 13MgH_2 + NdH_{2+x} + Mg_2NiH_x \quad (4)$$

After dehydrogenation, $Mg_2Ni$ formed, which shows the reversibility of $H_2$ storage in $Mg_2NiH_4$:

$$Mg_2NiH_x \Longleftrightarrow Mg_2Ni + x/2H_2 \quad (5)$$

### 3.2.2. *Kinetics*

Fig. 4 shows absorption and desorption curves at 350 °C for the second cycle (*i.e.* first reversible cycle). From now, the studied materials are the powder mixtures formed after the activation cycle and not the original alloys. These data are thus characterizing the mixture formed after the first activation step. Upon absorption, all mixtures are reacting rather fast with 80 % of reaction reached in less than 10 min. The capacities measured are around 4.5 %wt. The capacities are slightly lower for $NdNiMg_{15}$ (4.3 %wt.) and $GdCuMg_{15}$ (3.9 %wt.), which are still over 80 % of the theoretical capacities calculated from Mg content estimated with EDXS and taking into account $MgH_2$ and $Mg_2NiH_4$ contributions: 5.1%wt. and 4.9%wt. respectively. The desorption capacities are close to the absorptions ones, which shows the reversibility of the reaction. Desorption curves present different shapes and kinetics depending on the mixture used. $NdNiMg_{15}$ and $NdCu_{0.5}Ni_{0.5}Mg_{15}$ have fast kinetics, similar to the absorption curves. The three other materials have slower kinetics than during absorption. It is worth noting that the mixtures with slower kinetics are for mixtures with TM = Cu, using MT = Ni seems to provide better desorption kinetics to $RETMMg_{15}$ materials [12,18–22]. This observation must be due to the different catalytic effect of each TM on the desorption as well as the different kinetics for the reactions (3) and (5) involving the TM element.

Desorption with $GdCuMg_{15}$ mixture is slower than with $Nd_{0.5}Gd_{0.5}CuMg_{15}$, which is slower than reaction with $NdCuMg_{15}$. The catalytic effect of rare earth on Mg hydrogenation properties have been evidenced experimentally several times [23,24]. From the above comparisons it seems that Nd has a stronger catalytic effect on the desorption kinetics as compared to Gd. It should be noted here that $GdCuMg_{15}$ and $Nd_{0.5}Gd_{0.5}CuMg_{15}$ alloys had significantly higher contents of α-Mg phase (Table 1 and Fig. 2), which results in a less homogeneous distribution of TM and RE in the material and a lower efficiency of the catalytic effect of these elements.

In order to get more information on the reaction mechanisms, the kinetic data of Fig. 4 were linearized according to the following relation:

$$Ln(-ln(1-x)) = f(ln(t)) \quad (6)$$

According to Sharp and Hancock method, the data analysis is limited between 10 and 50 % of reaction in order to get a linear plot from equation (6). This limited reaction range is not greatly influenced by uncertainty in the initial conditions nor affected appreciably by particle

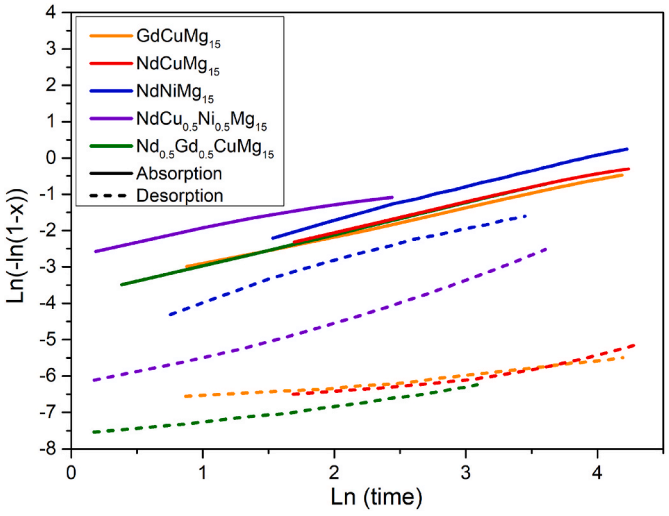


**Fig. 5.** Kinetic data of Fig. 4 linearized between 10 % and 50 % of reaction.

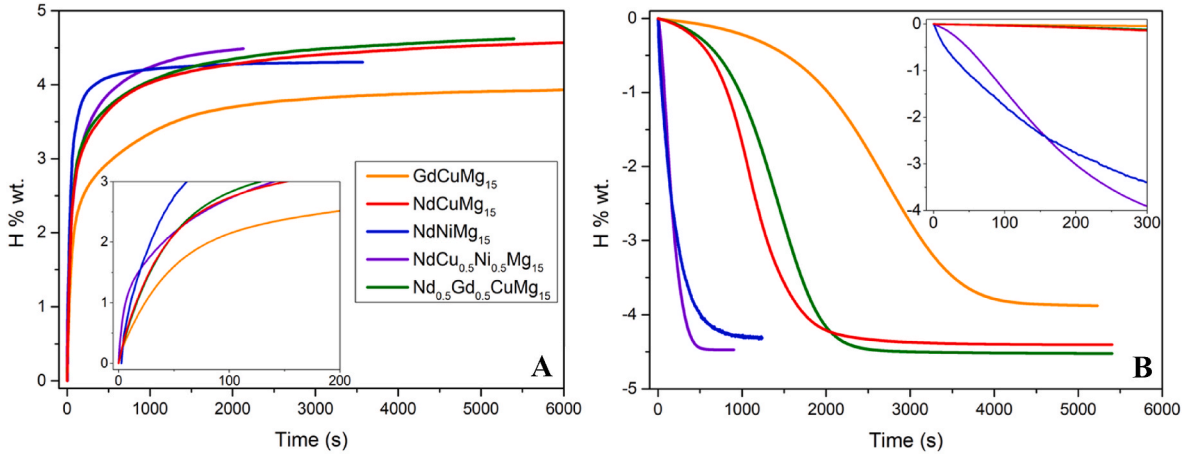


**Fig. 4.** Second cycle at 350 °C for the five studied materials: A- Absorption under 2000 kPa and B- desorption under 200 KPa of hydrogen.

**Table 2**
Reaction order deduced from the linearization method of Fig. 5.

| Alloy | Absorption | Desorption |
|---|---|---|
| $GdCuMg_{15}$ | 0,76 | 2,95 |
| $NdCuMg_{15}$ | 0,81 | 2,92 |
| $NdNiMg_{15}$ | 0,93 | 0,83 |
| $NdCu_{0,5}Ni_{0,5}Mg_{15}$ | 0,48 | 1,53 |
| $Nd_{0,5}Gd_{0,5}CuMg_{15}$ | 0,84 | 2,7 |

size distribution and other geometrical factors [25]. The resulting curves are assimilated to lines (Fig. 5) whose slopes n characterize the reaction mechanisms [25–27]. The n values obtained for each material are summarized in Table 2. Reaction order values close to 0.5 are related to reactions controlled by a diffusion process and values close to 1 are better described by the interface evolution (phase boundary). Absorption reaction with $NdCu_{0,5}Ni_{0,5}Mg_{15}$ has an order of 0.48 which indicates a diffusion controlled process. Absorption with other materials have values between 0.5 and 1, which indicates that both interface evolution and diffusion process influence the reaction kinetics. Except for $NdNiMg_{15}$, desorption reactions are based on completely different mechanisms than absorption. $NdNiMg_{15}$ present close reaction orders upon hydrogenation (0.93) and dehydrogenation (0.83) indicating similar mechanisms, mostly influenced by the interface propagation. In the case of $GdCuMg_{15}$, $NdCuMg_{15}$ and $Nd_{0,5}Gd_{0,5}CuMg_{15}$ the n value is close to 3, which corresponds to the Avrami-Erofeev model with a 3 dimensional propagation (competition between nucleation and 3D-growth in the volume). Desorption of $NdCu_{0,5}Ni_{0,5}Mg_{15}$ mixture gives an order of 1.5 that shows an influence of different mechanisms on the kinetics. In order to interpret better the kinetic data of this composition, two different sections could be analyzed independently: one between 10 % and 25 % and another between 25 % and 50 %. However, there is no certainty that the different mechanisms occur in such distinct timeframes.

### 3.2.3. *Thermodynamics*

Pressure-Composition-Temperature (PCT) diagrams for absorption and desorption reactions are showed for $NdCuMg_{15}$ and $NdNiMg_{15}$ on Fig. 6. It is visible on Fig. 6A' that there are at least two plateaus on the PCT curve of $NdCuMg_{15}$ for desorption reaction at 360 °C and 350 °C.

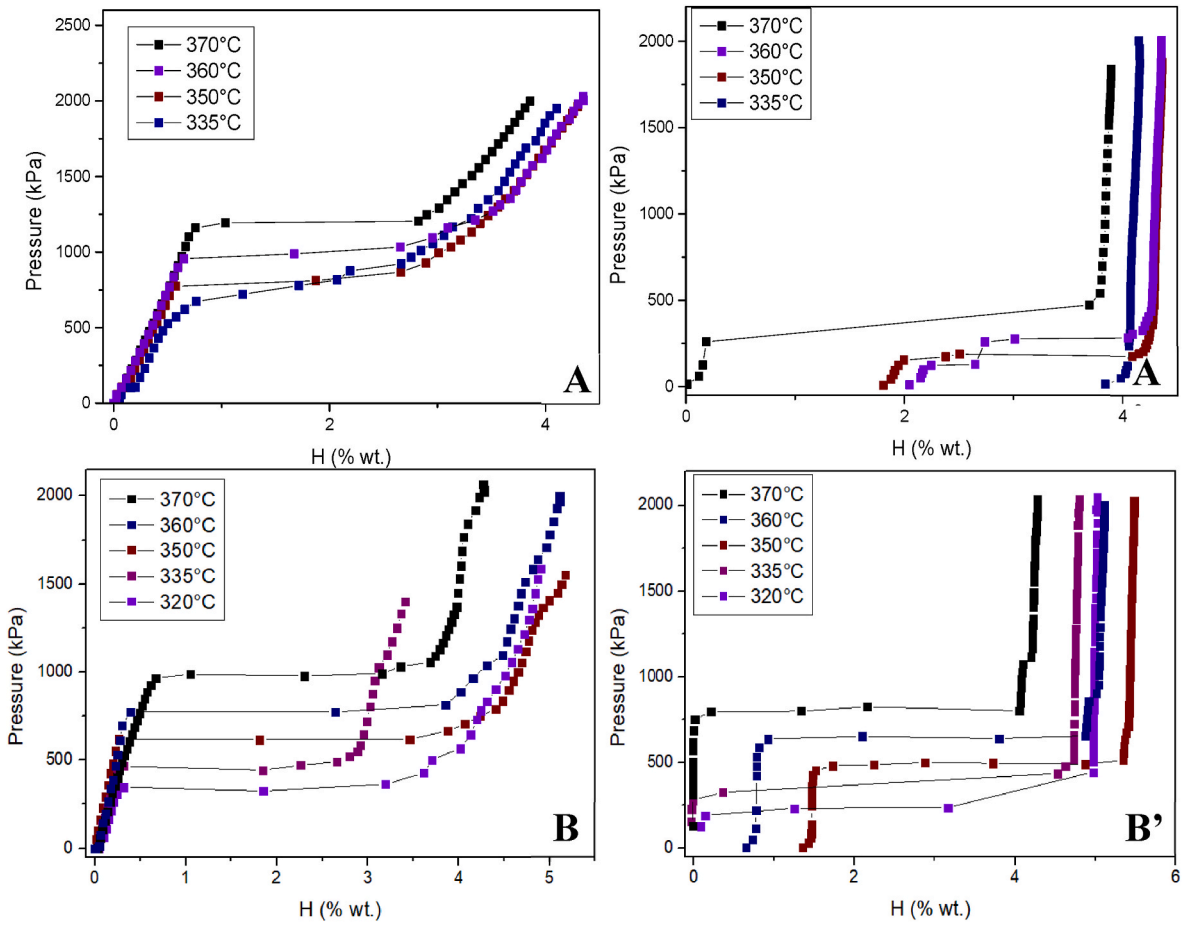


**Fig. 6.** PCT diagrams of A- $NdCuMg_{15}$ and B- $NdNiMg_{15}$. A and B for absorption, A′ and B′ for desorption.

**Table 3**
Ratio of $P^{eq}_{abs}$ over $P^{eq}_{des}$ calculated from PCT diagrams for relevant temperatures.

| Temperature (°C) | $GdCuMg_{15}$ | $NdCuMg_{15}$ | $NdNiMg_{15}$ | $NdCu_{0,5}Ni_{0,5}Mg_{15}$ | $Nd_{0,5}Gd_{0,5}CuMg_{15}$ |
|---|---|---|---|---|---|
| 320 | - | - | 1,5 | - | - |
| 335 | - | - | 1,2 | - | - |
| 350 | - | - | 1,2 | 1,6 | - |
| 360 | - | - | 1,2 | 1,4 | - |
| 370 | 2,5 | 2,5 | 1,2 | 1,3 | 2,4 |

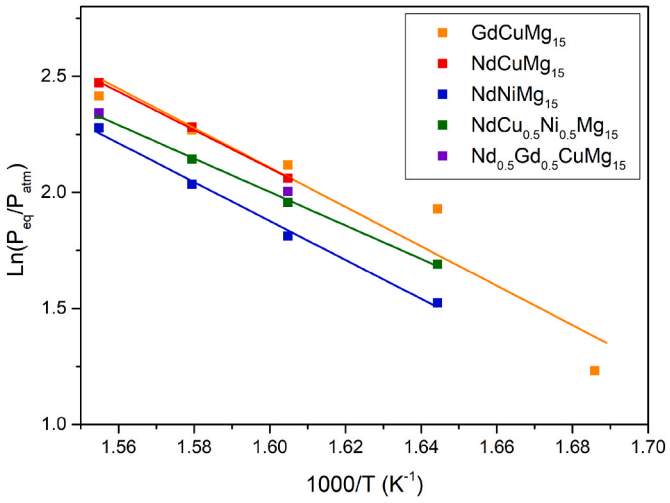


**Fig. 7.** Van't Hoff plots of the five studied materials for absorption reactions.

**Table 4**
Enthalpy and entropy of hydride formation deduced from Fig. 7.

| | Absorption | |
|---|---|---|
| Alloy (number of points used for regression) | ΔH (KJ/molH$_2$) | ΔS (J/K/molH$_2$) |
| GdCuMg$_{15}$ (5) | 70,5 | 129,7 |
| NdCuMg$_{15}$ (3) | 68,4 | 127,0 |
| NdNiMg$_{15}$ (5) | 69,7 | 127,1 |
| NdCu$_{0,5}$Ni$_{0,5}$Mg$_{15}$ (4) | 59,9 | 115,8 |

Each plateau correspond to reactions (2) and (3). In the case of NdCuMg$_{15}$ it is less easy to distinguish the reaction involving Mg$_2$Ni (equation (5)). It was possible to deduce the reaction hysteresis ($P^{eq}_{abs}$/$P^{eq}_{des}$) at some temperatures. Table 3 reports these values and shows differences among materials. NdCu$_{0.5}$Ni$_{0.5}$Mg$_{15}$ and NdNiMg$_{15}$ both present equivalent hysteresis at all temperatures (with a $P^{eq}_{abs}$ about 1.5 times higher than $P^{eq}_{des}$). For the three other materials, the ratio is 2.5 at 370 °C. The presence of Nickel does not only strongly affect the kinetics but also implies a smaller hysteresis between absorption and desorption. It can be seen on Fig. 5 that some experiments exhibit lower capacities for the same material, this is due to samples that were not fully dehydrogenated. The important information here lies in the plateau position. The capacity properties are discussed in section 3.b.ii with corresponding data.

PCT measurements at different temperatures allowed to draw the Van't Hoff plots of Fig. 7 and deduce the enthalpy and entropy variations reported in Table 4. These values are obtained from Van't Hoff relation:

$$ln\left(P^{eq} \Big/ P_{atm}\right) = \frac{\Delta H}{RT} - \frac{\Delta S}{R} \quad (4)$$

Where ΔH is the enthalpy variation (KJ/molH$_2$), ΔS is the entropy variation (J/K/molH$_2$), R the gas constant (8.314 J/mol/K), T the temperature (K) and $P^{eq}$ the equilibrium pressure (kPa).

The enthalpy values reported in Table 4 are all close to 70 kJ/molH$_2$, which is slightly below the value of 74 kJ/molH$_2$ known for formation of MgH$_2$ from pure Mg [28,29]. Only NdCu$_{0,5}$Ni$_{0,5}$Mg$_{15}$ present particularly low values of enthalpy and entropy as compared to other materials. The calculation for Nd$_{0,5}$Gd$_{0,5}$CuMg$_{15}$ material could not be done because only two meaningful points were obtained from PCT curves. It seems from these values that the different alloys present reduced enthalpies; the effect of each alloying element is however not easy do discriminate. The desorption enthalpies measured for the studied materials are actually closer to alloy materials than pure Mg. Indeed, Mg2NiH4 desorption enthalpy was reported to be 64 kJ/mol [30]. As a matter of comparison, intermetallics compounds deemed to have among the best desorption properties such as LaNi5, FeTi or NaAl have respective enthalpies of 31 kJ/mol, 31,5 kJ/mol and 40 kJ/mol respectively [31,32].

## 4. Conclusion

The microstructural and hydrogenation properties of five RE (Nd or Gd)-TM (Ni or Cu)–Mg$_{15}$ alloys have been studied. All materials presented a main phase of the NdNiMg$_{15}$-type, which is identified for the first time with Nd and Cu elements. It has been found that both RE and TM element can be substituted by other RE and TM elements respectively to form an intermediary compound. All alloys decomposed into binary (MgH$_2$, REH$_{2+x}$) or ternary (Mg$_2$NiH$_4$) hydrides under 2000 kPa of H$_2$ at 350 °C. The reversible hydrogenation kinetic (2nd cycle) was fast with 80 % of reaction reached in less than 10 min. The capacities measured are close to 4.5 % wt., which correspond to 80 % of the theoretical capacity. The kinetics of dehydrogenation reactions were significantly different for the five materials and faster desorption kinetics were observed for materials containing TM = Ni and RE = Nd. The presence of different alloying elements resulted in lowering the MgH$_2$ formation enthalpy in these alloys.

## Funding

Mitacs Globalink funded this work through agreement number IT25655. The authors thank Mitacs Globalink for their support.

## Declaration of competing interest

The authors declare that they have no known competing financial interests or personal relationships that could have appeared to influence the work reported in this paper.

## Appendix A. Supplementary data

Supplementary data to this article can be found online at https://doi.org/10.1016/j.ijhydene.2023.10.294.

## References

[1] Baum ZJ, Diaz LL, Konovalova T, Zhou QA. Materials research directions towards a green hydrogen economy : a review. ACS Omega 2022;7:32908–35.
[2] Dawood F, Anda M, Shafiullah GM. Hydrogen production for energy: an overview. Int J Hydrogen Energy 2020;45:3847–69. https://doi.org/10.1016/j.ijhydene.2019.12.059.
[3] Shang Y, Pistidda C, Gizer G, Klassen T, Dornheim M. Mg-based materials for hydrogen storage. J Magnesium Alloys 2021. https://doi.org/10.1016/j.jma.2021.06.007.
[4] Oelerich W, Klassen T, Bormann R. Metal oxides as catalysts for improved hydrogen sorption in nanocrystalline Mg-based materials. J Alloys Compd 2001;315:237–42. https://doi.org/10.1016/S0925-8388(00)01284-6.
[5] Huot J, Liang G, Boily S, Van Neste A, Schulz R. Structural study and hydrogen sorption kinetics of ball-milled magnesium hydride. J Alloys Compd 1999;293:495–500. https://doi.org/10.1016/S0925-8388(99)00474-0.
[6] Denys RV, Zavaliy IY, Paul-Boncour V, Berezovets VV, Koval'chuk IV, Riabov AB. New Mg-Mn-Ni alloys as efficient hydrogen storage materials. Intermetallics 2010;18:1579–85. https://doi.org/10.1016/j.intermet.2010.04.011.
[7] Charbonnier V, Asano K, Kim H, Sakaki K. Hydrogenation properties of Mg 83.3 Cu 7.2 Y 9.5 with long period stacking ordered structure and formation of polymorphic γ-MgH 2. Inorg Chem 2020;59:0–11. https://doi.org/10.1021/acs.inorgchem.0c02080.
[8] Kalinichenka S, Röntzsch L, Riedl T, Gemming T, Weißgärber T, Kieback B. Microstructure and hydrogen storage properties of melt-spun Mg-Cu-Ni-Y alloys. Int J Hydrogen Energy 2011;36:1592–600. https://doi.org/10.1016/j.ijhydene.2010.10.099.
[9] Liu J, Zou C, Wang H, Ouyang L, Zeng M, Zhu M. Enhancing effect of LPSO phases on hydrogen ab- and desorption kinetics of Mg94Cu4Y2 alloy. Cailiao Yanjiu Xuebao/Chinese J Mater Res 2016;30:248–54. https://doi.org/10.11901/1005.3093.2015.189.
[10] Kalisvaart WP, Harrower CT, Haagsma J, Zahiri B, Luber EJ, Ophus C, et al. Hydrogen storage in binary and ternary Mg-based alloys: a comprehensive

experimental study. Int J Hydrogen Energy 2010;35:2091–103. https://doi.org/10.1016/j.ijhydene.2009.12.013.
[11] Couillaud S, Gaudin E, Andrieux J, Gorsse S, Gayot M, Bobet JL. Study of the hydrogenation mechanism of LaCuMg 8 ternary phase: the decomposition induces kinetics improvement. Int J Hydrogen Energy 2012;37:11824–34. https://doi.org/10.1016/j.ijhydene.2012.05.025.
[12] Si TZ, Liu YF, Zhang QA. Hydrogen storage properties of the supersaturated Mg12YNi solid solution. J Alloys Compd 2010;507:489–93. https://doi.org/10.1016/j.jallcom.2010.07.214.
[13] Shibata K, Tanaka K, Kurumatani K, Nishida Y, Takeshita HT. Thermodynamic evaluation for formation of MgCu2 from MgH2 and Cu. Pacific Rim Int. Congr. Adv. Mater. Process. 2013;1:221. https://doi.org/10.1007/978-3-319-48764-9_28.6.
[14] Bobet JL, Lesportes P, Roquefere JG, Chevalier B, Asano K, Sakaki K, et al. A preliminary study of some "pseudo-AB2" compounds: RENi4 Mg with RE = La, Ce and Gd. Structural and hydrogen sorption properties. Int J Hydrogen Energy 2007;32:2422–8. https://doi.org/10.1016/j.ijhydene.2006.11.031.
[15] Al Asmar E, Tencé S, Bobet JL, Ourane B, Nakhl M, Zakhour M, et al. The Mg-rich phase NdNiMg15: structural and magnetic properties. Inorg Chem 2018;57:14152–8. https://doi.org/10.1021/acs.inorgchem.8b02007.
[16] Couillaud S, Gaudin E, Weill F, Gomez S, Stan C, Planté D, et al. Structure of a new ternary compound with high magnesium content, so-called Gd13Ni9Mg78. Acta Mater 2012;60:4144–51. https://doi.org/10.1016/j.actamat.2012.04.012.
[17] Ourane B, Gaudin E, Lu YF, Zouari R, Salah A Ben, Bobet JL. The new ternary intermetallic NdNiMg5: hydrogen sorption properties and more. Mater Res Bull 2015;61:275–9. https://doi.org/10.1016/j.materresbull.2014.10.026.
[18] Ouyang LZ, Yang XS, Zhu M, Liu JW, Dong HW, Sun DL, et al. Enhanced hydrogen storage kinetics and stability by SynergisticEffects ofin SituFormed CeH2.73and Ni in CeH2.73-MgH2-NiNanocomposites. J Phys Chem C 2014;118:7808–20.
[19] Yao P, Jiang Y, Liu Y, Wu C, Chou KC, Lyu T, et al. Catalytic effect of Ni@rGO on the hydrogen storage properties of MgH2. J Magnesium Alloys 2020;8:461–71. https://doi.org/10.1016/j.jma.2019.06.006.
[20] Varin RA, Czujko T, Wasmund EB, Wronski ZS. Catalytic effects of various forms of nickel on the synthesis rate and hydrogen desorption properties of nanocrystalline magnesium hydride (MgH2) synthesized by controlled reactive mechanical milling (CRMM). J Alloys Compd 2007;432:217–31. https://doi.org/10.1016/j.jallcom.2006.05.129.
[21] Hanada N, Ichikawa T, Fuji H. Catalytic effect of nanoparticle 3d-transition metals on hydrogen storage properties inMagnesium hydride MgH2Prepared by mechanical milling. J Phys Chem B 2005;109:7188–94.
[22] Shang CX, Bououdina M, Song Y, Guo ZX. Mechanical alloying and electronic simulations of (MgH2+M) systems (M=Al, Ti, Fe, Ni, Cu and Nb) for hydrogen storage. Int J Hydrogen Energy 2004;29:73–80. https://doi.org/10.1016/S0360-3199(03)00045-4.
[23] Pezat M, Darriet B, Hagenmuller P. A comparative study of magnesium-rich rare earth based alloys for hydrogen storage. J Less-Common Met 1980;74:427–34.
[24] Jin RS, Zhang J, Zhou XJ, Pan SX, He JH, Chen JN, et al. Microstructures and hydrogen storage properties of Mg-Y-Zn rare earth magnesium alloys with different Zn content: experimental and first-principles studies. Mater Today Commun 2022;32. https://doi.org/10.1016/j.mtcomm.2022.104119.
[25] Hancock JD, Sharp JH. Method of comparing solid-state kinetic data and its application to the decomposition of kaolinite, brucite, and BaCO3. J Am Ceram Soc 1972;55:74–7. https://doi.org/10.1111/j.1151-2916.1972.tb11213.x.
[26] Perrin S. Modélisation de la cinétique de transformations non isothermes et (ou) non isobares. Application à la déshydroxylation de la kaolinite et à la réduction de l' octooxyde de triuranium par l' hydrogène. ECOLE NATIONALE SUPERIEURE DES MINES DE SAINT-ETIENNE; 2002.
[27] Sharp JH, Brindley GW, Narahari Hachar BN. Equations, numerical data for some commonly used solid state reaction. J Am Ceram Soc 1966;19. https://doi.org/10.1111/j.1151-2916.1966.tb13289.x.
[28] Pivak Y, Schreuders H, Dam B. Thermodynamic properties, hysteresis behavior and stress-strain analysis of MgH2 thin films, studied over a wide temperature range. Crystals 2012;2:710–29. https://doi.org/10.3390/cryst2020710.
[29] Zhang J, Li Z, Wu Y, Guo X, Ye J, Yuan B, et al. Recent advances on the thermal destabilization of Mg-based hydrogen storage materials. RSC Adv 2019;9:408–28.
[30] Zhu M, Lu Y, Ouyang L, Wang H. Thermodynamic tuning of Mg-based hydrogen storage alloys: a review. Materials 2013 Oct;6(10):4654–74. https://doi.org/10.3390/ma6104654.
[31] Dornheim M. Thermodynamic properties of metal hydrides. Thermodynamics - interaction studies - solids, Liquids, Gases 10.5772/21662.
[32] Sakintuna B, Lamari-Darkrim F, Hirscher M. Metal hydride materials for solid hydrogen storage: a review. Int J Hydrogen Energy 2007;32:1121–40. https://doi.org/10.1016/j.ijhydene.2006.11.022.